Bidirectional PWM Converter Integrating Cell Voltage Equalizer Using Series-Resonant Voltage Multiplier for Series-Connected Energy Storage Cells

Masatoshi Uno, *Member, IEEE*, and Akio Kukita

Abstract—In conventional energy storage systems using series-connected energy storage cells such as lithium-ion battery cells and supercapacitors (SCs), an interface bidirectional converter and cell voltage equalizer are separately required to manage charging/discharging and ensure years of safe operation. In this paper, a bidirectional PWM converter integrating cell voltage equalizer is proposed. This proposed integrated converter can be derived by combining a traditional bidirectional PWM converter and series-resonant voltage multiplier (SRVM) that functionally operates as an equalizer and is driven by asymmetric square wave voltage generated at the switching node of the converter. The converter and equalizer can be integrated into a single unit without increasing the switch count, achieving not only system-level but also circuit-level simplifications. Open-loop control is feasible for the SRVM when operated in discontinuous conduction mode (DCM), meaning the proposed integrated converter can operate similarly to conventional bidirectional converters. An experimental charge-discharge cycling test for six SCs connected in series was performed using the proposed integrated converter. The cell voltage imbalance was gradually eliminated by the SRVM while series-connected SCs were cycled by the bidirectional converter. All the cell voltages were eventually unified, demonstrating the integrated functions of the proposed converter.

Index Terms— Battery, equalizer, integrated converter, series-resonant voltage multiplier, supercapacitor, voltage imbalance.

I. INTRODUCTION

Secondary battery-based energy storage plays an important role in various electrical systems, from small-scale portable electronic devices to large-scale systems, including electric vehicles and grid-connected applications. Lithium-ion batteries are among the most promising secondary battery technologies because of their superior energy density to other traditional battery chemistries. Supercapacitors (SCs) are also key emerging electrical energy storage devices, which offer excellent cycle life performance as well as high power capability, since their energy storage mechanism is not dependent on chemical reactions. SC applications have been expanding from hybrid energy storage systems, which involve SCs operating as high-power energy buffers, to alternative energy storage sources to conventional secondary batteries [1]. Although their inferior energy density performance is considered a disadvantage, their performance has been steadily increasing. In addition, the commercialization of lithium-ion capacitors (LICs), a hybrid SC combining features of lithium-ion batteries and conventional SCs to achieve both high-power capability and higher energy density [2], [3], has been launched, driving expectations of the penetration of SC technologies used in various applications.

In general, energy storage cells/modules (hereafter, simply 'cells') need to be connected in series to form a string to meet system voltage requirements. The voltages of individual series-connected cells gradually become imbalanced due to characteristic mismatches in terms of capacity/capacitance, self-discharge rate, and internal impedance. The temperature gradient in energy storage modules/systems comprising numerous cells connected in series is another major cause of voltage imbalance, because the self-discharge rate is significantly temperature-dependent. If cell voltages are mismatched, some cells with higher (or lower) voltages might be over-charged (or over-discharged) during the charging (or discharging) process because cells are charged (or discharged) in series. Energy storage cells, particularly lithium-ion cells, must be operated within a safety boundary to ensure years of safe operation otherwise resulting in accelerated aging and increased risks of hazardous consequences triggering an explosion in the worst case scenario. Accordingly, for energy storage modules/systems to operate safely and properly, cell voltage equalization techniques to eliminate and/or preclude cell voltage imbalance are crucial.

Various kinds of voltage equalization techniques and architectures have been proposed and demonstrated for series-connected lithium-ion cells and SCs. Two representative equalization architectures, cell-to-cell and string-to-cell, are shown in Fig. 1. The cell-to-cell equalization architecture shown in Fig. 1(a) is the most straightforward approach using

The authors are with Japan Aerospace Exploration Agency, Ibaraki 305-8505, Japan (e-mail: uno.masatoshi@jaxa.jp; kukita.akio@ jaxa.jp).

multiple cell-to-cell equalizers that are basically bidirectional converters, such as buck-boost converters [4]–[9] and switched capacitor converters [10]–[18], via which power is transferred between adjacent cells for equalization. However, these equalizers are prone to complexity because the numbers of switches and converters grow with the number of cells connected in series. Furthermore, since the power transfer is limited only between adjacent cells, the energy of cells may have to traverse several converters and cells if the string comprises numerous cells connected in series, collectively resulting in a significant power conversion loss.

In string-to-cell architecture, the whole string energy is directly transferred to the least charged cell with the lowest voltage to effectively equalize cell voltages. Equalizers using a single isolated converter with selection switches [19]–[22] are categorized into this architecture, and can dramatically reduce passive component counts. However, not only is the required switch count still proportional to the number of cells, an intelligent management system is also indispensable to determine and select the target cell with the lowest voltage in the string. Another major string-to-cell equalizer is a forward or flyback converter with a multi-winding transformer [23]–[26]. Although the switch count can be reduced to one or two, the strict parameter-matching requirement for multiple secondary windings is considered a design hurdle and impairs the modularity (or extendibility) [27], [28]. Many other equalization topologies using multiple converters [29], [30], multiphase converters [31], transformers [32]–[34] and multi-winding transformers [35], etc. [27], [28] have been proposed, but still face common issues of the increased switch count and/or the existence of a multi-winding transformer.

Single-switch equalizers using multi-stacked buck-boost converters can be built without a multi-winding transformer and provide both simple circuitry and good modularity [36]. However, the disadvantage is that the inductor count is proportional to the number of cells connected in series, likely resulting in increased volume and cost, particularly for large-scale systems comprising numerous cells. Meanwhile, voltage equalizers using an inverter with voltage multipliers can be configured with neither a multi-winding transformer nor multiple inductors [37], [38]. In addition to the reduced magnetic component count, two-switch topologies are feasible, thus achieving simplified circuitry, good modularity, and miniaturized design.

In general, all the aforementioned equalizers are externally added to the string, as illustrated in Fig. 1, and the bidirectional converter and equalizer(s) operate individually and independently. In other words, conventional energy storage systems require two functional components of the bidirectional converter and equalizer(s) to manage the string. If these two functional components can be integrated into a single unit, energy storage systems would be simplified by reducing the number of components. An equalization charger capable of not only charging but also equalizing cell voltages has been proposed for small-scale energy storage systems [39]. Although

the energy storage system can be simplified by integrating a charger and equalizer into a single unit, this equalization charger cannot be used for discharging the string because it is basically a charger or unidirectional converter. Bidirectional converters with an equalization function have been proposed [40], whereby the filter inductor in conventional converters is replaced with a multi-winding transformer having multiple secondary windings tied to individual cells for equalization. Although this converter can handle both charging/discharging and equalization, the existence of the multi-winding transformer would considerably hinder design flexibility and modularity, like conventional equalizers [27], [28].

In this paper, a bidirectional PWM converter integrating voltage equalizer for series-connected energy storage cells is proposed. The proposed integrated converter can be derived by combining a traditional bidirectional PWM converter and a series-resonant voltage multiplier (SRVM) that functionally operates as a voltage equalizer and is driven by an asymmetric square wave voltage generated at a switching node of the PWM converter. The bidirectional converter and voltage equalizer can be integrated into a single unit without increasing switch count, thus realizing not only system-level but also circuit-level simplifications. The rest of this paper is organized as follows. Section II outlines the key elements required for the proposed integrated converter, followed by the derivation procedure and a discussion of major benefits of the integrated converter. Section III presents a detailed operational analysis, including the establishment of operational criteria and the derivation of dc equivalent circuits of the SRVM and integrated converter to explain the voltage equalization mechanism. In Section IV, the experimental results of a charge/discharge cycling test using a prototype of the integrated converter performed for six SCs connected in series are presented to demonstrate the efficacy of the proposed concept.

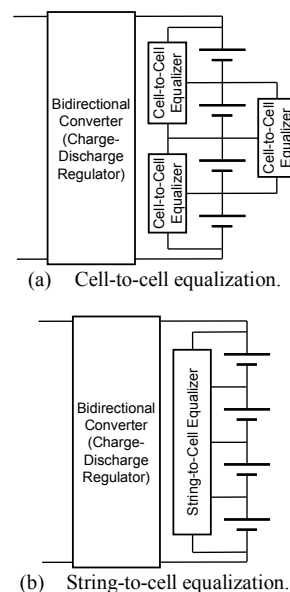(a)　Cell-to-cell equalization.

(b)　String-to-cell equalization.

Fig. 1.　Representative equalization architectures with interface bidirectional converter: (a) cell-to-cell and (b) string-to-cell equalization architectures.

II. INTEGRATED CONVERTER

A. Architecture of Integrated Converter

The schematic architecture of the proposed integrated converter is depicted in Fig. 2. Similar to the conventional equalization architecture using a string-to-cell equalizer shown in Fig. 1(b), the proposed integrated converter comprises two functional elements of the bidirectional converter and string-to-cell equalizer. The major difference is that some key circuit components are shared by the two functional elements without increasing the total circuit component count, and their operations in the proposed integrated converter are interdependent, as will be discussed in detail later. Conventional equalization architectures shown in Fig. 1, conversely, require a bidirectional converter and equalizer(s) separately, meaning that equalizers are physically and functionally independent of the bidirectional converter. This contrast suggests potential system-level simplification by integrating two functional elements into a single unit.

B. Key Elements for Integrated Converter

The proposed integrated bidirectional converter can be derived by combining a traditional PWM converter and series-resonant voltage multiplier (SRVM) as shown in Figs. 3 and 4, respectively. Although Fig. 3 depicts unidirectional PWM converters using a diode, these can be readily modified to bidirectional converters by replacing the diode with a switch. The SRVM functionally operates as a voltage equalizer, while all traditional PWM converters can be used as bidirectional converters.

The SRVM is basically a combination of a series-resonant tank and voltage multiplier, and is driven by a square wave voltage v_{SN}. Sinusoidal current i_{Lr} flows in the series-resonant tank, whereupon this current is transferred to the secondary side (i_{VM}) and rectified in the voltage multiplier. When an ac current/voltage wave is applied to the voltage multiplier, voltages of smoothing capacitors C_{out1}–C_{out4} are automatically unified. The detailed voltage equalization mechanism of the voltage multiplier will be explained in Section III-E.

Resonant tanks, not only series-resonant but also other resonant tanks, are generally driven by a symmetric square wave voltage generated by half- or full-bridge inverters. Meanwhile, as shown in the insets of Fig. 3, asymmetric square wave voltages are generated at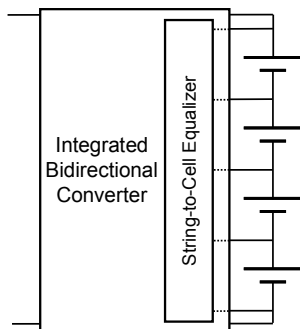 switching nodes of traditional PWM converters. In the proposed integrated converters, the asymmetric square wave voltage produced at a switching node of a PWM converter is exploited as v_{SN} (designated in Fig. 3) to drive the SRVM so that the PWM converter and SRVM can be integrated without increasing the switch count. There are two switching nodes in the SEPIC, Zeta, and Ćuk converters, and either can be used. Although only nonisolated PWM converters are treated in this paper, any other converters, including isolated and resonant types, would also be usable, provided that there is a switching node producing an asymmetric square wave voltage.

C. Derived Integrated Converter

A derived integrated converter based on a PWM buck converter with the SRVM is shown in Fig. 5, as a representative topology for four cells B_1–B_4 connected in series. The unidirectional buck converter shown in Fig. 3(a) is modified to be a bidirectional synchronous converter by replacing the diode with a switch Q_L. The PWM synchronous converter operates in

Fig. 2.　Architecture of proposed integrated converter.

(a) Buck converter.

(b) Boost converter.

(c) Buck-boost converter.

(d) SEPIC.
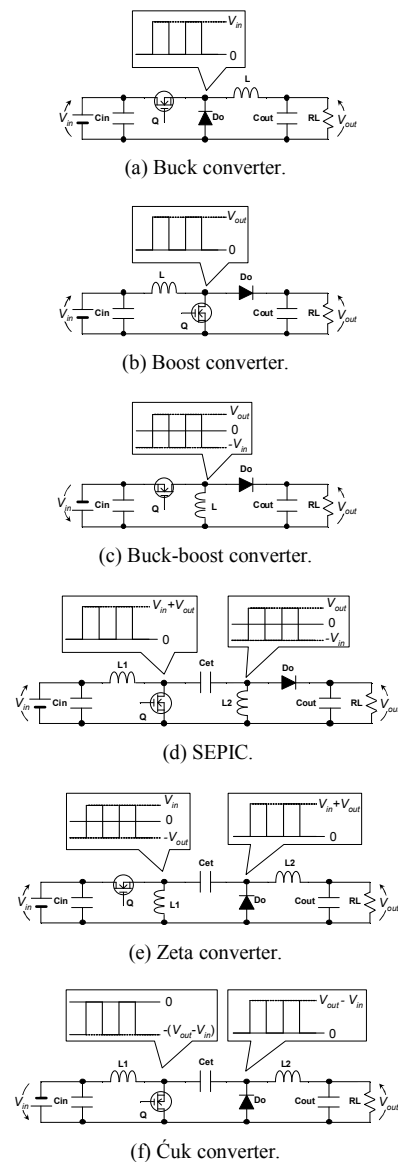
(e) Zeta converter.

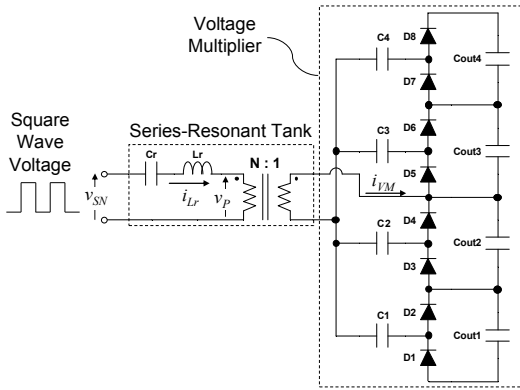(f) Ćuk converter.

Fig. 3.　Non-isolated PWM converters.

Fig. 4. Series-resonant voltage multiplier (SRVM).

step-down and -up modes during charging and discharging, respectively. Meanwhile, the SRVM is connected to the switching node of the synchronous converter, and the asymmetric square wave voltage generated at the switching node is utilized to drive the SRVM. The smoothing capacitors C_{out1}–C_{out4} in the SRVM are connected to B_1–B_4 in parallel to equalize cell voltages.

The SRVM can perform equalization during both charging and discharging, provided the asymmetric square wave voltage is generated at the switching node. Similar to conventional voltage equalizers using a voltage multiplier, the equalization current is preferentially supplied to the least charged cell with the lowest voltage in the string, and the voltage imbalance is gradually eliminated as the preferential current supply progresses [37]–[39]. During the charging period, the string is mainly charged by the bidirectional converter, while equalization current is preferentially supplied from the SRVM to the least charged cell in the string, virtually boosting the charging rate for the least charged cell. During the discharging period, conversely, the string is discharged by the bidirectional converter, while the SRVM still preferentially supplies equalization current to the least charged cell, decreasing the

discharging rate of the least charged cell. In other words, the larger the equalization current, the more quickly the cell voltages can be equalized by virtually increasing/decreasing the charging/discharging rates.

D. Major Benefits

In the conventional equalization architectures shown in Fig. 1, a bidirectional converter and equalizer(s) are separately necessary. Conversely, in the proposed integrated converter architecture, the bidirectional converter and equalizer can be integrated into a single unit, allowing system-level simplification. Circuit-level simplification is also feasible because no additional switch is required for the integration. The switch count is considered a good index to represent the circuit complexity because each switch requires multiple ancillary components, including a driver IC, auxiliary power supply, and passive devices. The total switch count collectively required for the integrated converter is only two―the SRVM itself is essentially a switchless circuit―, whereas the conventional systems shown in Fig. 1 require two switches for the bidirectional converter and at least one switch for even the simplest equalizer [36]. Furthermore, the required magnetic component count (including the filter inductor L in the bidirectional converter) is only a few, allowing more compact design than conventional equalizers using numerous magnetic components.

As will be discussed in Section III-C, no control is necessary to limit currents in the SRVM under a desired current level, provided it is operated in discontinuous conduction mode (DCM). Accordingly, the bidirectional converter in the proposed integrated converter can operate identically to conventional bidirectional converters; only the duty cycle is controlled to regulate the charging/discharging current and string voltage, according to the input-to-output voltage relationship.
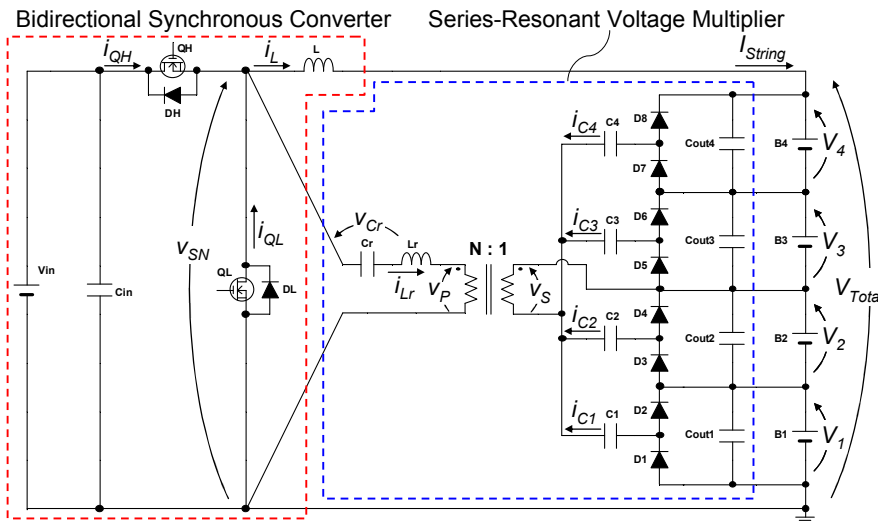

Fig. 5. Proposed integrated converter based on bidirectional synchronous converter with series-resonant voltage multiplier.

Table I. Comparison for equalization techniques.

Topology	Equalization Architecture	Simplicity*	Volume**	Modularity***	Remark
Buck-Boost Converter [4]–[8]	Cell-to-Cell	P	P	E	Inductor count is $\propto n$
Switched Capacitor Converter [10]–[18]	Cell-to-Cell	P	G	E	-
Isolated Converter with Selection Switches [19]–[22]	String-to-Cell or Cell-to-String	P	E or G	G	Target cell determination is necessary
Multi-Winding Trasformer [23]–[26]	String-to-Cell	G	E	P	-
Flyback Converter [32], [33]	String-to-Cell or Cell-to-String	P	P	G	Transformer count is $\propto n$
Single-Switch Multi-Stacked Converters [36]	String-to-Cell	G	P	G	Inductor count is $\propto n$
Double-Switch Voltage Multiplier [37], [38]	String-to-Cell	G	G	G	-
Single-Switch Voltage Multiplier [39]	String-to-Cell (Integrated)	E	G	G	Integration feasible for charger only
Multi-Winding Transformer-Integrated Converter [40]	String-to-Cell or Cell-to-String (Integrated)	E or P	E	P	Multi-winding transformer is necessary for integration
Proposed Integrated Converter	String-to-Cell (Integrated)	E	G	G	-

† E: Excellent, G: Good, P: Poor   *Switch count "in the equalizer" is E: zero, G: a few, P: $\propto n$.
† n is the number of cells connected in series   **Passive component counts is E: a few, G: $\propto n$ capacitors, P: $\propto n$ magnetic components.
† Smoothing capacitors are excluded for comparison   ***Circuit can be extended with E: modular design, G: minor design change, P: redesigning multi-winding transformer.

With the proposed integrated converter, cell voltages are equalized by the SRVM that is driven by an asymmetric square wave voltage generated at the switching node of the bidirectional converter, and therefore, voltage equalization performance is influenced only by the bidirectional converter. In other words, as long as the bidirectional converter operates stably and generates the asymmetric square wave voltage at its switching node, the SRVM can properly perform equalization in any applications.

In general, the required current for equalization is rather smaller than charging/discharging currents; in float charging applications, for example, an equalization current hundred times smaller than a charging current is considered sufficient to preclude the occurrence of voltage imbalance [11], [41], although the optimum equalization current rate would be dependent on applications. Therefore, the bidirectional converter and equalizer(s) should be designed separately and optimally considering their respective power requirements. In a conventional integrated converter [40], the magnetic component is shared, which would make it somewhat cumbersome for the optimum design. In the proposed integrated converter, conversely, despite the integration, the bidirectional converter and SRVM can be separately designed, allowing optimal designs for the respective elements.

Since the SRVM operation is linked to that of the bidirectional converter, equalization currents are always supplied to cells in the string, regardless of whether cell voltages are imbalanced; supplying equalization currents for voltage-balanced cells is meaningless and results in needless power conversion loss in the SRVM. The required equalization currents are generally rather smaller than charging/discharging currents as mentioned above [11], [41], implying the loss associated with the SRVM would be very minor. If the minor loss in the SRVM needs to be eliminated to maximize the overall system efficiency, it is advisable to insert a relay or switch to the input of the resonant tank to disable the SRVM.

E. Comparison with Conventional Equalizers

Proposed integrated converter and representative conventional equalizers are compared and arbitrary rated from the perspectives of equalization architecture, circuit simplicity, volume, and modularity (or extendibility), as shown in Table I; rating criterion are specified at the bottom of the table. Cell-to-cell equalization architectures offer the best modularity, though ratings in other aspects are relatively low. Equalization techniques utilizing a multi-winding transformer would potentially be compact, but the existence of a multi-winding transformer is likely to be a serious issue in terms of the modularity and design difficulty, as mentioned in Section I, especially for applications requiring numerous cells connected in series. Meanwhile, the integrated architectures would offer not only the system-level simplification thanks to the integration but also the simplest circuitries at reasonable volume. Although there is no one-fits-all solution, the proposed integrated converter is considered to be an attractive easy-to-design solution as it achieves system-level and circuit-level simplifications at reasonable volume with no need for a multi-winding transformer.

III. OPERATING ANALYSIS

In this section, the proposed integrated converter is analyzed for charging direction only, but the operation during discharging can be understood and analyzed similarly. For clarity, the overall operation of the integrated converter is analyzed first, followed by detailed analysis of the SRVM. Finally, the DCM operational criteria for the whole integrated converter are discussed.

A. Consideration of Operation Mode of Series-Resonant Voltage Multiplier

As discussed in the previous section, the SRVM is driven by the asymmetric square wave voltage generated at a switching node of the PWM converter. In general, the duty cycle in PWM converters varies according to the relationship between input

and output voltages, indicating that the duty cycle of the asymmetric square wave voltage for the SRVM also varies. Accordingly, the operation of the SRVM should desirably be independent on duty cycle variations. In addition, since outputs of the SRVM are connected to energy storage cells that are basically constant voltage sources, currents in the SRVM need to be controlled or limited to within desired levels.

In the proposed integrated converter, the SRVM is designed to operate in discontinuous conduction mode (DCM), whereby currents can be kept nearly constant, even with open-loop control, as will be mathematically revealed in Section III-C. In addition to the inherent constant current characteristic, DCM operation can be ensured even with an asymmetric square wave voltage containing duty cycle variations, rendering it optimal for the proposed integrated converter.

B. Overall Operation

The analysis and discussion performed hereafter are based on the premise that the magnetizing inductance of the transformer is large enough so that a magnetizing current can be ignored to simplify the operation analysis. The key operation waveforms and current flow directions during charging when the voltage of B_1, V_1, is the lowest in the string are shown in Figs. 6 and 7, respectively, while the current flow paths in Fig. 7 are illustrated assuming currents in the voltage multiplier are buffered by smoothing capacitors C_{out1}–C_{out4}. There are six operation modes provided the SRVM operates in DCM, whereby no currents flow in Modes 3 and 6. As specified in Fig. 6, waveforms can be classified into two groups of converter-related and SRVM-related waveforms, allowing separate analyses for the bidirectional converter and SRVM. The operation of the
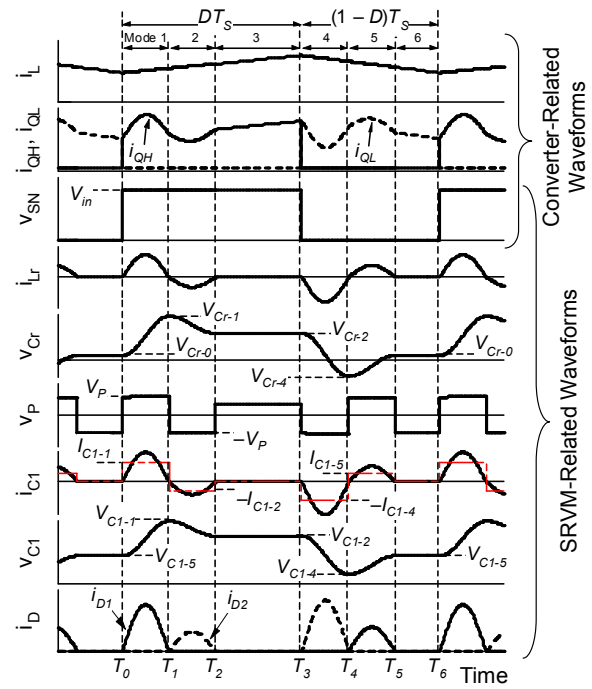
Fig. 6. Operation waveforms of proposed integrated converter during charging when V_1 is the lowest in the string.

bidirectional converter in the proposed integrated converter is almost identical to that of a traditional buck converter. Hence, in the following sections, the operational analysis is performed mainly focusing on the SRVM.

Before detailing each operation mode, the major parameters are defined as follows: the characteristic impedance of the resonant tank Z_0, the characteristic angular frequency ω_0, and
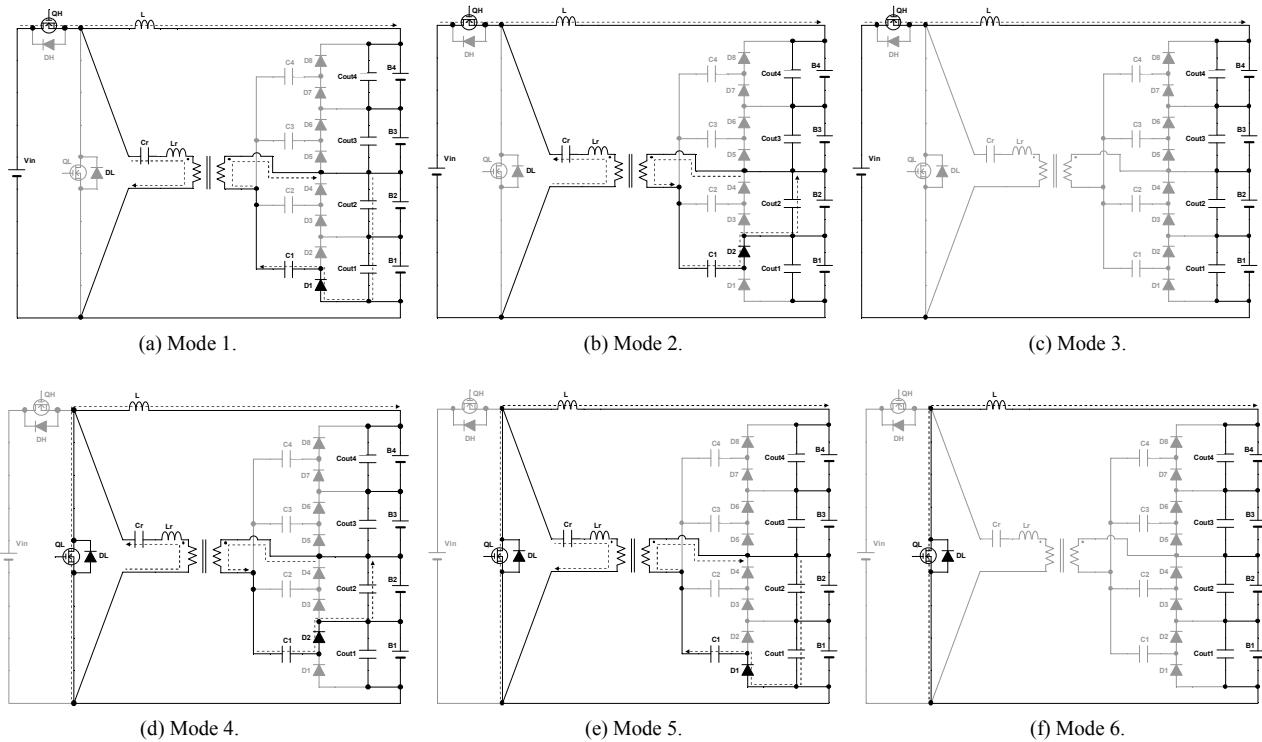
(a) Mode 1.   (b) Mode 2.   (c) Mode 3.

(d) Mode 4.   (e) Mode 5.   (f) Mode 6.

Fig. 7. Operation modes during charging when V_1 is the lowest.

resonant angular frequency ω_r are given by

$$Z_0 = \sqrt{\frac{L_r}{C_r}}, \ \omega_0 = \frac{1}{\sqrt{L_r C_r}}, \ \omega_r = \sqrt{{\omega_0}^2 - \gamma^2} \ . \tag{1}$$

where L_r is the inductance of L_r, and C_r is the capacitance of C_r, and

$$\gamma = \frac{R}{2L_r}, \tag{2}$$

R is the sum of the resistive components in the current flow path (i.e. resistances of the series-resonant tank, primary and secondary transformer windings, and components in the voltage multiplier).

i) Mode 1 ($T_0 < t < T_1$):

The first mode, Mode 1, begins as the upper switch Q_H is turned on, and the voltage of the switching node v_{SN} is at a high level equal to the input voltage of V_{in}. The filter inductor current i_L linearly increases while the sinusoidal current of the resonant inductor L_r, i_{Lr}, starts flowing through the resonant tank and is superimposed on the current of the upper switch i_{QH}. i_{Lr} is transferred to the secondary side, whereupon D_1, a lower diode connected to the least charged cell of B_1, conducts to charge C_1 in the voltage multiplier.

i_{Lr} and v_{Cr} in Mode 1, i_{Lr-1} and v_{Cr-1}, are expressed as

$$i_{Lr-1}(t) = \frac{V_{in} - V_{Cr-0} - V_P}{Z_0} e^{-\gamma t} \sin \omega_r t \ , \tag{3}$$

$$v_{Cr-1}(t) = (V_{in} - V_P) - (V_{in} - V_{Cr-0} - V_P) e^{-\gamma t} \cos \omega_r t \ , \tag{4}$$

where V_P is the primary winding voltage that will be expressed by (27) in Section III-E. At $t = T_1$, v_{Cr} is

$$v_{Cr}(T_1) = (V_{in} - V_P) + (V_{in} - V_{Cr-0} - V_P) e^{-\gamma T_r/2} = V_{Cr-1} \ . \tag{5}$$

where T_r is the resonant period.

ii) Mode 2 ($T_1 < t < T_2$):

The integrated converter starts operating in Mode 2, as the direction of i_{Lr} is reversed. Current paths in the converter are identical to those in Mode 1, and i_L is still linearly increasing. Meanwhile, C_1 in the voltage multiplier is being discharged through D_2, an upper diode connected to B_1. The polarity of the transformer primary winding voltage is also reversed, but its amplitude is the same as that in Mode 1 because of the operational symmetry of the voltage multiplier. i_{Lr} and v_{Cr} in Mode 2, i_{Lr-2} and v_{Cr-2}, are

$$i_{Lr-2}(t) = \frac{V_{in} - V_{Cr-1} + V_P}{Z_0} e^{-\gamma(t-T_1)} \sin \omega_r (t - T_1), \tag{6}$$

$$v_{Cr-2}(t) = (V_{in} + V_P) - (V_{in} - V_{Cr-1} + V_P) e^{-\gamma(t-T_1)} \cos \omega_r (t - T_1). \tag{7}$$

At $t = T_2$, v_{Cr} is

$$v_{Cr}(T_2) = (V_{in} + V_P) + (V_{in} - V_{Cr-1} + V_P) e^{-\gamma T_r/2} = V_{Cr-2} \ . \tag{8}$$

iii) Mode 3 ($T_2 < t < T_3$):

As i_{Lr} reaches zero, the operation shifts to Mode 3, whereby no currents flow in the SRVM, although the input voltage remains at the high level of V_{in}. As can be seen in Fig. 7(c), this operation mode is exactly identical to the on-period of a traditional buck converter.

iv) Mode 4 ($T_3 < t < T_4$):

By turning off Q_H, Mode 4 begins, and i_L starts linearly decreasing and flowing through the freewheeling diode of D_L or the synchronous switch Q_L, similar to an off-period of a traditional buck converter. v_{SN} in this mode is at a low level of nearly zero, and i_{Lr} flows back toward the switching node and is superimposed on the current of the lower switch i_{QL}. In the voltage multiplier, C_1 is being discharged through D_2, similar to Mode 2. i_{Lr} and v_{Cr} in Mode 4, i_{Lr-4} and v_{Cr-4}, are expressed as

$$i_{Lr-4}(t) = \frac{-V_{Cr-2} + V_P}{Z_0} e^{-\gamma(t-T_3)} \sin \omega_r (t - T_3), \tag{9}$$

$$v_{Cr-4}(t) = V_P - (-V_{Cr-2} + V_P) e^{-\gamma(t-T_3)} \cos \omega_r (t - T_3). \tag{10}$$

v_{Cr} at $t = T_4$ is

$$v_{Cr}(T_4) = V_P + (-V_{Cr-2} + V_P) e^{-\gamma T_r/2} = V_{Cr-4} \ . \tag{11}$$

v) Mode 5 ($T_4 < t < T_5$):

In Mode 5, i_{Lr} becomes positive, and D_1 in the voltage multiplier conducts to charge C_1. The current flow paths in the converter are identical to those in Mode 4, and i_L keeps linearly decreasing. Similar to previous operation modes, i_{Lr} and v_{Cr} in Mode 5, i_{Lr-5} and v_{Cr-5}, are

$$i_{Lr-5}(t) = \frac{-V_{Cr-4} - V_P}{Z_0} e^{-\gamma(t-T_4)} \sin \omega_r (t - T_4), \tag{12}$$

$$v_{Cr-5}(t) = -V_P - (-V_{Cr-4} - V_P) e^{-\gamma(t-T_4)} \cos \omega_r (t - T_4). \tag{13}$$

At $t = T_5$, v_{Cr} equals to V_{Cr-0} and is expressed as

$$v_{Cr}(T_5) = -V_P + (-V_{Cr-4} - V_P) e^{-\gamma T_r/2} = V_{Cr-0} \ . \tag{14}$$

vi) Mode 6 ($T_5 < t < T_6$):

The last mode, Mode 6, is identical to the off-period of a traditional buck converter; i_L keeps linearly declining while no currents flow in the SRVM.

The converter-related waveforms resemble those of a traditional PWM buck converter, and can be divided into two; Modes 1–3 and 4–6, which represent on- and off-periods, respectively. Although the discontinuous sinusoidal current wave of i_{Lr} is superimposed on the waveforms of i_{QH} and i_{QL}, the inductor current i_L remains purely triangular, indicating that the voltage conversion ratio of a traditional buck converter (i.e. $V_{Total} = DV_{in}$ for charging) holds even in the integrated converter.

Meanwhile, in the voltage multiplier, currents flow through only C_1, D_1, and D_2, which are connected to the least charged cell of B_1, whereas no currents flow through other components. The average diode current of D_1 or D_2 is equal to an equalization current supplied to B_1 because the average current of C_1 must be zero under a steady-state condition. This tendency can be generalized; an equalization current flows toward the least charged cell(s) only. The voltage multiplier is analyzed in detail in Section III-E.

C. Modeling for Current Characteristic of Series-Resonant Voltage Multiplier

From the operational symmetry between Modes 1–3 and 4–6,

$$V_{Cr-1} + V_{Cr-4} = V_{Cr-0} + V_{Cr-2} = V_{in} \ . \tag{15}$$

Substitution of (15) into (5), (8), (11), and (14) produces

$$\begin{cases} V_{Cr-0} = \dfrac{1}{1+e^{-\gamma T_r}}\left\{(V_{in}-V_P)e^{-\gamma T_r} - 2V_P e^{\frac{-\gamma T_r}{2}} - V_P\right\} \\ V_{Cr-1} = \dfrac{1}{1+e^{-\gamma T_r}}\left\{(V_{in}+V_P)e^{-\gamma T_r} + V_{in}e^{\frac{-\gamma T_r}{2}} + (V_{in}-V_P)\right\} \\ V_{Cr-2} = \dfrac{1}{1+e^{-\gamma T_r}}\left\{V_P e^{-\gamma T_r} + 2V_P e^{\frac{-\gamma T_r}{2}} + (V_{in}+V_P)\right\} \\ V_{Cr-4} = \dfrac{1}{1+e^{-\gamma T_r}}\left\{-V_P e^{-\gamma T_r} - V_{in}e^{\frac{-\gamma T_r}{2}} + V_P\right\} \end{cases} \quad (16)$$

By substituting (16) into (3), (6), (9), (12),

$$\begin{cases} i_{Lr-1}(t) = -i_{Lr-4}(t) = \dfrac{e^{-\gamma t}}{Z_0\left(1+e^{-\gamma T_r}\right)}\left(V_{in}+2V_P e^{\frac{-\gamma T_r}{2}}\right)\sin\omega_r t \\ i_{Lr-2}(t) = -i_{Lr-5}(t) = \dfrac{e^{-\gamma t}}{Z_0\left(1+e^{-\gamma T_r}\right)}\left(-V_{in}e^{\frac{-\gamma T_r}{2}}+2V_P\right)\sin\omega_r t \end{cases} \quad (17)$$

These equations verify that i_{Lr} in Modes 1–2 is symmetrical to that in Modes 4–5.

i_{Lr} is transferred to the secondary side in the form of i_{VM}, whereupon i_{VM} is rectified in the voltage multiplier and supplied to cells as a dc current. The rectified i_{VM}, I_{VM}, can be obtained by integrating $|i_{VM}|$ over the switching period of T_S, as

$$\begin{aligned} I_{VM} &= \frac{1}{T_S}\int_0^{T_S} N|i_{Lr}(t)|dt \\ &= \frac{N\omega_S\omega_r}{\pi Z_0\left(\gamma^2+\omega_r^2\right)}\frac{V_{in}\left(1+e^{-\gamma T_r/2}\right)^2 - 2V_P\left(1-e^{-\gamma T_r}\right)}{1+e^{-\gamma T_r}} \end{aligned} \quad (18)$$

where N is the transformer turns ratio, and ω_S is the angular switching frequency. This equation implies that I_{VM} declines slightly with increasing V_P. If R is negligible and γ can be considered zero in the ideal case, (18) can be simplified to

$$I_{VM} \approx \frac{2N\omega_S V_{in}}{\pi Z_0\omega_r}. \quad (19)$$

This equation verifies that I_{VM} under a given condition in the ideal case is constant, even at a fixed frequency, and is independent of V_P or cell voltages. Thus, by designing the SRVM based on (18) and (19), currents in the SRVM can automatically be limited to within desired levels, even without feedback control.

D. DCM Operation Criteria for Series-Resonant Voltage Multiplier

For each operation mode to exist, i_{Lr} in Modes 1 and 5 must be positive, and vice versa in Modes 2 and 4. From (3), (6), (9), and (12),

$$\begin{cases} V_{in}-V_{Cr-0}-V_P > 0 & (Mode\,1) \\ V_{in}-V_{Cr-1}+V_P < 0 & (Mode\,2) \\ -V_{Cr-2}+V_P < 0 & (Mode\,4) \\ -V_{Cr-4}-V_P > 0 & (Mode\,5) \end{cases} \quad (20)$$

If these criteria are violated, no currents in the SRVM flow in each mode, similar to Modes 3 and 6—in a practical case, a little current flows through the magnetizing inductance of the transformer, which has been ignored for the sake of simplicity, even when these criteria are violated. Meanwhile, currents in the voltage multiplier must be blocked in Mode 3 and 6. To this end, V_P must exceed $v_{SN} + v_{Cr}$ in Modes 3 and 6;

$$\begin{cases} V_{in}-V_{Cr-2}-V_P < 0 & (Mode\,3) \\ -V_{Cr-0}+V_P > 0 & (Mode\,6) \end{cases}. \quad (21).$$

E. Operation of Voltage Multiplier and Equalization Mechanism

The operational analysis of the voltage multiplier is performed for the case shown in Fig. 7; V_1 is the lowest in the string. To simply the analysis, the current C_1 in each operation mode is averaged as I_{C1-m} (where m corresponds to each operation mode number), as designated in Fig. 6. The voltages of C_1 at the end of each mode, V_{C1-m}, which are also designated in Fig. 6, are expressed as

$$\begin{cases} V_{C1-1} = \dfrac{V_P}{N}-V_D-(V_1+V_2)-I_{C1-1}r \\ V_{C1-5} = \dfrac{V_P}{N}-V_D-(V_1+V_2)-I_{C1-5}r \end{cases}, \quad (22)$$

$$\begin{cases} V_{C1-2} = -\dfrac{V_P}{N}+V_D-V_2+I_{C1-2}r \\ V_{C1-4} = -\dfrac{V_P}{N}+V_D-V_2+I_{C1-4}r \end{cases}, \quad (23)$$

where V_1 and V_2 are the cell voltages of B_1 and B_2, V_D is the forward voltage drop of diodes, and r is the collective resistance of the current path in the voltage multiplier. The voltage variation of C_1 over a switching cycle, ΔV_{C1}, can be yielded by summing all of V_{C1-m} given by (22) and (23), as

$$\begin{aligned} \Delta V_{C1} &= V_{C1-1}-V_{C1-2}-V_{C1-4}+V_{C1-5} \\ &= 4\frac{V_P}{N}-2V_1-4V_D-2\frac{f_r}{f_S}I_{VM}r \end{aligned}, \quad (24)$$

where I_{VM} is the rectified secondary current of i_{VM}, expressed as

$$\begin{aligned} I_{VM} &= \frac{\left(I_{C1-1}+I_{C1-2}+I_{C1-4}+I_{C1-5}\right)\dfrac{T_r}{2}}{T_S} \\ &= \frac{f_S}{2f_r}\left(I_{C1-1}+I_{C1-2}+I_{C1-4}+I_{C1-5}\right) \end{aligned}. \quad (25)$$

This equation means that I_{VM} is equal to the rectified I_{C1-m} averaged over a switching period of T_S. ΔV_{C1} can be expressed differently as

$$\Delta V_{C1} = \frac{Q}{C_1} = \frac{1}{2}\frac{I_{VM}}{C_1 f_S}. \quad (26)$$

From (24)–(26),

$$\frac{2}{N}V_P = V_1 + 2V_D + \frac{I_{VM}}{2}R_{eq}, \quad (27)$$

where

$$R_{eq} = \frac{1}{2C_1 f_S}+\frac{2f_r}{f_S}r. \quad (28)$$

Although (27) and (28) have been yielded only for B_1, similar equations for other cells can be obtained by the same analytical procedure.

From (27), a dc equivalent circuit of the voltage multiplier can be obtained as shown in Fig. 8. The derived dc equivalent circuit of the voltage multiplier in the proposed integrated
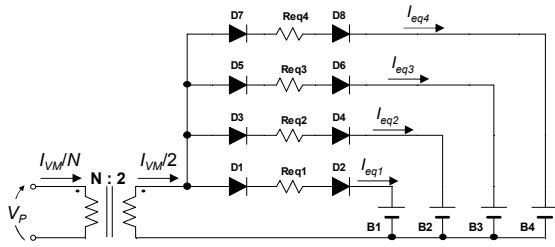
Fig. 8. DC equivalent circuit of voltage multiplier.

converter is identical to that of conventional equalizers using a voltage multiplier [37], [38]; all cells are connected to the secondary winding of the ideal transformer with a turn ratio of N:2 through respective equivalent resistors and diodes, and an equalization current of $I_{VM}/2$ is distributed to cells. The equalization current preferentially flows toward the least charged cell having the lowest voltage, and all the cell voltages eventually become uniform. Despite the similar equivalent circuit, the value of R_{eq} differs and is dependent on how the voltage multiplier is driven; the series-resonant inverter operating in DCM is used in the proposed integrated converter, while voltage multipliers in conventional equalizers of [37] and [38] are driven by a half-bridge inverter and parallel-/series-parallel-resonant inverter, respectively. Detailed consideration about the impact of parameter mismatch on equalization performance can be found in the previous work [38].

F. DC Equivalent Circuit of Integrated Converter

Since the proposed integrated converter is basically the combination of the PWM converter and SRVM, a dc equivalent circuit for the proposed integrated converter as a whole can be derived from (18) with the combination of equivalent circuits of the PWM converter and SRVM (see Fig. 8), as shown in Fig. 9, in which an ideal multi-winding transformer with the turn ratio of N:2:2:2:2 is introduced for the cells to be connected in series. The PWM converter is equivalently illustrated as an ideal transformer having the turn ratio of 1:D. The primary winding of the SRVM's equivalent circuit is tied to the PWM converter's input through a current source of $I_{in-SRVM}$ in order to extract the current of I_{VM}/N.

This dc equivalent circuit contains no high-frequency switching components, dramatically reducing the simulation burden and time. Therefore, the derived dc equivalent circuit would be a powerful tool to briefly investigate the impact of parameter mismatching, such as component tolerance and capacitance mismatch, on equalization performance. The result of simulation-based charge/discharge cycling will be shown and compared with the experimental result in Section IV.

G. Operation Criterion for Integrated Converter

The resonant and switching frequencies, f_r and f_S, need to be determined considering duty cycle variation so that the SRVM always operates in DCM. Both the on- and off-periods (DT_S and $(1 − D)T_S$, respectively) must exceed the resonant period T_r. From this relationship, the criterion for D is yielded as
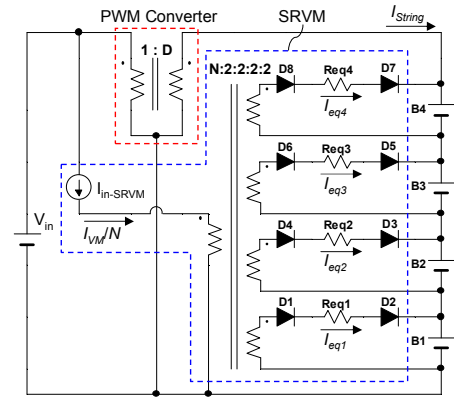

Fig. 9. DC equivalent circuit of integrated converter as a whole.

$$1 - \frac{f_S}{f_r} > D > \frac{f_S}{f_r} . \qquad (29)$$

IV. EXPERIMENTAL RESULTS

A. Prototype and Experimental Setup

Given that SC modules comprising of six cells connected in series are readily available on a market, the proposed integrated converter was designed and built for six SCs in series for the experimental demonstration. Prototypes of the bidirectional converter and SRVM were separately built, as shown in Fig. 10, to measure the individual characteristic of the SRVM. As discussed in Section II-D, the required equalization current is generally rather smaller than that for charging/discharging; an equalization current 1/100 of charging current is considered sufficient for float charging applications [11], [41]. However, in order to expedite the experiments, the SRVM was designed so that the equalization current supplied to each cell under a

(a)   Bidirectional converter.
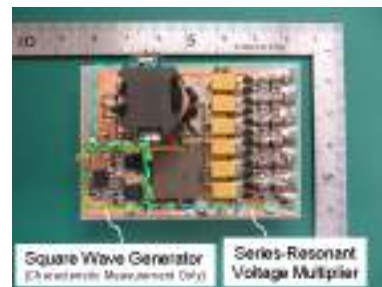
(b)   Series-resonant voltage multiplier.

Fig. 10.   Photographs of (a) bidirectional converter and (b) series-resonant voltage multiplier for six cells connected in series.

Table II. Component values used for prototypes.

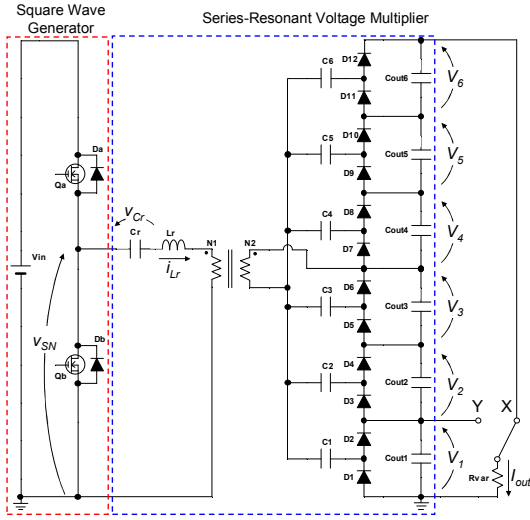|	Component	Value
Synchronous Bidirectional Converter	L	220 μH
	Q_H, Q_L	N-Ch MOSFET, IR7855, R_{on} = 15 mΩ
	D_H, D_L	Schottky Diode, 15MQ040N, V_D = 0.43 V
	C_{in}	Aluminum Electrolytic Capacitor, 660 μF
Series-Resonant Voltage Multiplier	D_1–D_{12}	Schottky Diode, 15MQ040N, V_D = 0.43 V, R_D = 64.6 mΩ
	C_1–C_6	Tantalum Capacitor, 100 μF, 35 mΩ
	C_{out1}–C_{out6}	Ceramic Capacitor, 200 μF
	C_r	Ceramic Capacitor, 22 nF, 60 mΩ
	L_r	5.6 μF, 19 mΩ
	Transformer	N_1:N_2 = 25:4, L_{kg} = 3.4 μH, L_{mg} = 722 μH $R_{primary}$ = 560 mΩ, $R_{secondary}$ = 45.9 mΩ

Fig. 11. Experimental setup for characteristic measurement for series-resonant voltage multiplier.

voltage-balanced condition—each cell receives one-sixth of I_{VM}/2 (see (19) and (20)) under the voltage-balanced condition—was approximately one-tenth of the charging current of 1.0 A (see Section IV-C). The component values used for the prototypes are listed in Table II.

An experimental setup used for the characteristic measurement for the SRVM is shown in Fig. 11. Symmetric square wave voltage was produced at f_S = 100 kHz by the square wave generator, which was a half-bridge inverter with V_{in} = 24 V. Energy storage cells were removed, while voltages of V_1–V_6 were sustained by C_{out1}–C_{out6} alone. Current flow paths under voltage-balanced and -imbalanced conditions were emulated by selecting the intermediate tap of X and Y, respectively, through which an output current I_{out} was drawn; with the tap X selected, currents flow through all the components in the voltage multiplier, while only C_1, D_1, and D_2 (except for smoothing capacitors) are in operation when the tap Y is selected, emulating the voltage-imbalanced condition. As the voltage multiplier always receives the equalization current of I_{VM}/2, as explained in Section III-E (see Fig 8), I_{out} under the voltage-balanced and -imbalanced conditions are I_{VM}/12 and I_{VM}/2, respectively.

B. Characteristic of Series-Resonant Voltage Multiplier

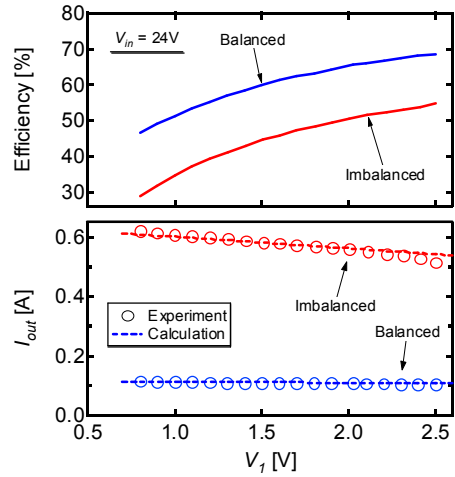The measured current characteristics and efficiencies of the

Fig. 12. Measured characteristics of series-resonant voltage multiplier.

SRVM as a function of V_1 are shown in Fig. 12, while theoretical current characteristics calculated based on (18) are also shown for comparison. Experimental and calculated current characteristics correlated well, verifying the current model obtained in Section III-C. The current characteristics under the voltage-balanced condition were virtually constant, whereas those under voltage-imbalanced conditions declined slightly with increasing V_1. The non-ideal constant current characteristics under voltage-imbalanced condition are attributable to the increased resistance due to current concentration, as implied by (18) and (19). Currents in the voltage multiplier uniformly flow through all of C_1–C_6 and D_1–D_{12} under the voltage-balanced condition, whereas those under the voltage-imbalanced condition tend to concentrate in C_1, D_1, and D_2, virtually increasing the resistance of the voltage multiplier.

The dominant loss factor is considered diode voltage drops taking a significant portion of V_1–V_6 that were lower than 2.5 V—V_1–V_6 correspond to cell voltages in a practical use. The measured efficiencies consistently increased with V_1, as the
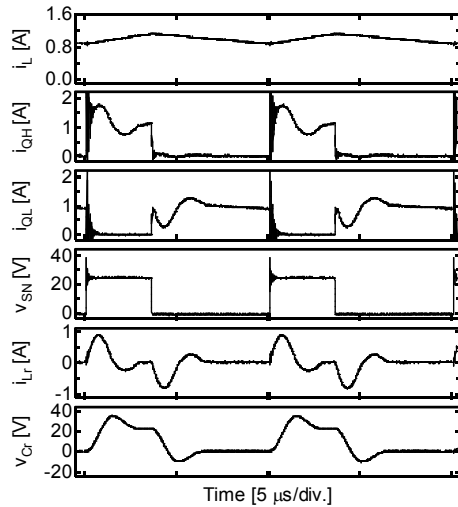

Fig. 13. Measured key waveforms at V_{Total} = 8.0 V and V_1 = 0.7 V during charging.

portion taken by diode voltage drops decreased. The inferior efficiency characteristic under the voltage-imbalanced condition is attributable to the current concentration that caused an increased Joule loss in the voltage multiplier. This measured efficiency trend is considered basically independent on main's dc voltage (i.e. V_{in} in Fig. 11 or the input voltage of the bidirectional converter in a practical use) because the SRVM outputs for cells and its efficiency is chiefly dependent on a cell voltage and diode voltage drop. Although not efficient, these measured efficiencies are considered acceptable in many applications because a required current for equalization is generally rather smaller than that for charging/discharging, as mentioned in Section II-D—the loss associated with the equalization would be very minor compared with that for the main converter.

C. Charge-Discharge Cycling Experiment

Six SCs each with a capacitance of 1500 F at a rated charge voltage of 2.5 V were used for the cycling experiment, and they were neither brand-new nor screened to minimize any nonuniformity in cell characteristics. The prototypes shown in Fig. 10 were combined by cables, and operated at f_S = 100 kHz to perform a charge-discharge cycling test from an initially-voltage-imbalanced condition, whereby V_1–V_6 were imbalanced within the range 0.7–1.6 V. The series-connected SCs were charged with a constant current–constant voltage (CC–CV) charging scheme of 1.0 A–15 V (2.5 V/cell) at V_{in} = 24 V, and were discharged to a 50-Ω resistor at a constant voltage of 22.7 V. Individual cell voltages, the total voltage of the string V_{Total}, and the string current I_{String} were measured, while cycling was repeated for three cycles.

Measured key operation waveforms at V_{Total} = 8.0 V and V_1 = 0.7 V during charging are shown in Fig. 13. Similar to the theoretical waveforms shown in Fig. 6, i_L was a triangular wave, while discontinuous sinusoidal current of i_{Lr} flowed as v_{SN} swung.

The experimental charge-discharge cycling profiles are shown in Fig. 14. During the first charging period, V_2–V_6 uniformly increased, while V_1 increased more rapidly, implying that the SRVM preferentially supplied an equalization current for B_1 having the lowest voltage in the string. After V_{Total} reached the CV charging voltage level of 15 V, I_{String} was tapered and V_{Total} was maintained at 15 V, whereas some cells were over-charged beyond 2.5 V because of the cell voltage imbalance. The voltage imbalance still gradually disappeared, even during the CV charging period, since the bidirectional converter was operated in synchronous mode and the string energy was redistributed to the cells through the SRVM. After the integrated converter had been switched to discharging, V_{Total} as well as cell voltages started decreasing. The cells were still being equalized during discharging, verifying that the SRVM can properly equalize during both charging and discharging; the standard deviation of the cell voltages consistently decreased during both charging and discharging.

The voltage imbalance was further eliminated in the second and third cycles. The standard deviation bottomed during the
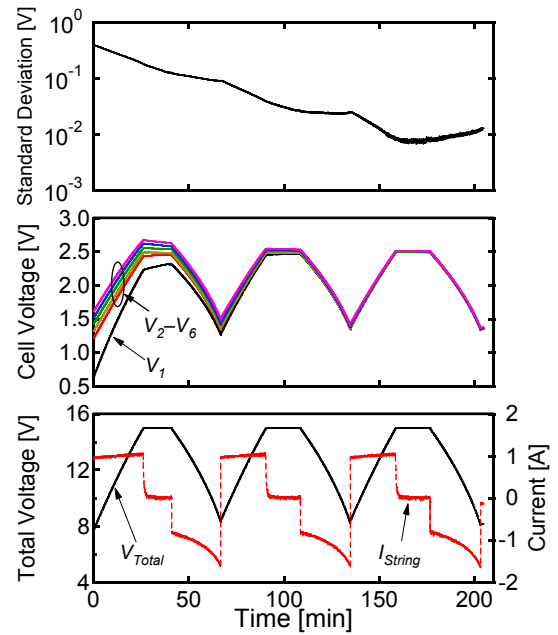

Fig. 14. Experimental charge-discharge cycling profiles of six SCs connected in series cycled by integrated converter.

CV charging period in the third cycle, followed by a slight increase during the discharging period. This slight increase in the standard deviation is attributable to a minor mismatch in capacitance of the SCs, with which SC voltages are naturally slightly imbalanced as they are charged/discharged—the capacitance mismatch is one of the major causes of voltage imbalance, as mentioned in Section I. During the CV charging period, I_{String} was tapered to be nearly zero, causing no voltage imbalance originating from the minor capacitance mismatch. In other words, the SC voltages were simply equalized during the CV charging period, reducing the standard deviation even with the existence of the minor capacitance mismatch. In the subsequent discharging period, on the other hand, SC voltages tended to be slightly imbalanced due to the minor capacitance mismatch, resulting in the slight increase in the standard deviation.

At the end of the cycling experiment, the standard deviation of cell voltages decreased down to approximately 10 mV, demonstrating the equalization performance of the proposed integrated converter.

D. Simulation Verification

A simulation-based charge-discharge cycling using the derived dc equivalent circuit shown in Fig. 9 was also performed under the same conditions as the experiments; R_{eq} was determined to be 364 mΩ based on (28). To briefly investigate the equalization performance under a capacitance-mismatched condition, the capacitance of B_3 was intentionally lowered by 10%—the capacitances of B_3 was 1350 F while others were still 1500 F.

The simulation cycling profiles are shown in Fig. 15. Even under the capacitance-mismatched condition, cell voltage profiles showed a good agreement with those in the experiment
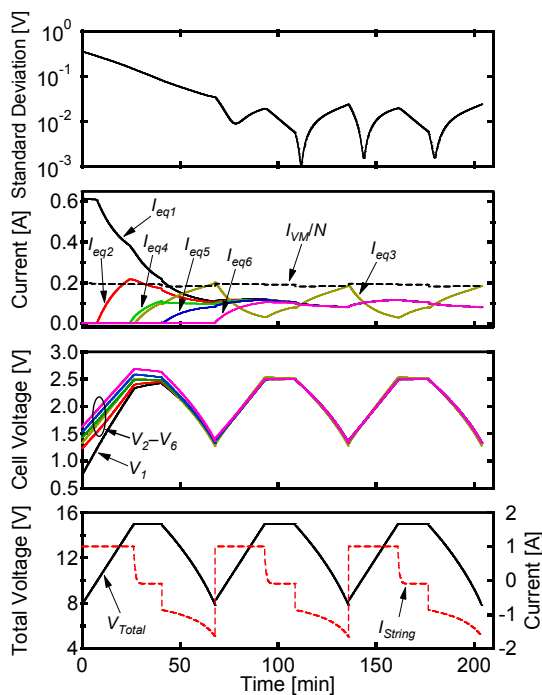
Fig. 15. Simulation charge-discharge cycling profiles of six SCs connected in series cycled by integrated converter.

shown in Fig. 14, successfully verifying the derived dc equivalent circuit. As charging/discharging progressed in the first cycle, cells received equalization currents one after the other, and the standard deviation consistently decreased. In the second and third cycles, on the other hand, all the cells received equalization currents, and the standard deviation fluctuated due to the capacitance mismatch. Similar to the experimental result shown in Fig. 14, the standard deviation increased during discharging periods as cell voltages tended to be slightly imbalanced due to the capacitance mismatch. Since the capacitances of B_3 was lower than the others, V_3 tended to be higher and lower during charging and discharging periods, respectively. Accordingly, the equalization current supplied to B_3, I_{eq3}, differed from others so that all the cell voltages were equalized during cycling.

In general, the larger the capacitance mismatch and charge/discharge currents, the greater will be the voltage imbalanced caused by cycling. Hence, equalizers should be properly designed with considering capacitance mismatch and cycling conditions so that cell voltages are adequately balanced even during cycling. The derived dc equivalent circuit would help investigating equalization performance under mismatched conditions and therefore be a useful tool for properly designing the equalizer.

V. CONCLUSIONS

A bidirectional PWM converter integrating a cell voltage equalizer has been proposed in this paper. The proposed integrated converter is basically the combination of a traditional bidirectional PWM converter and SRVM that functionally performs cell voltage equalization. An asymmetric square wave

voltage generated at the switching node of a converter is exploited to drive the SRVM, hence the SRVM itself is a switchless circuit. The two functional elements (i.e. bidirectional converter and equalizer) can be integrated into a single unit without increasing the switch count, hence realizing system- and circuit-level simplifications.

The operational analysis was mainly performed for the SRVM, since the fundamental operation of the bidirectional converter in the proposed integrated converter is basically identical to that of conventional converters. Detailed operational analysis revealed the inherent constant current characteristic of the SRVM, and hence currents in the SRVM can be automatically limited to within desired levels, even without feedback control.

An experimental charge-discharge cycling test using the proposed integrated converter was performed for six SCs connected in series from an initially-voltage-imbalanced condition. The voltage imbalance was gradually eliminated by the SRVM during both charging and discharging while the string was cycled by the bidirectional converter. The cell voltages were eventually unified at the end of the experimental cycling, demonstrating the integrated functions of the proposed converter.

REFERENCES

[1] M. Uno and K. Tanaka, "Accelerated charge-discharge cycling test and cycle life prediction model for supercapacitors in alternative battery applications," *IEEE Trans. Ind. Electron.*, vol. 59, no. 12, Dec. 2012, pp. 4704–4712.

[2] S. M. Lambert, V. Pickert, J. Holden, X. He, and W. Li, "Comparison of supercapacitor and lithium-ion capacitor technologies for power electronics applications," in Proc. *Power Electron. Machines and Drives*, 2010, Apr. 2010, pp. 1–5.

[3] M. Uno and K. Tanaka, "Spacecraft electrical power system using lithium-ion capacitors," *IEEE Trans. Aerosp. Electron. Syst.*, vol. 49, no. 1, Jan. 2013, pp. 175–188.

[4] K. Nishijima, H. Sakamoto, and K. Harada, "A PWM controlled simple and high performance battery balancing system," in Proc. *IEEE Power Electron. Spec. Conf.*, Jun. 2000, pp. 517–520.

[5] Y. S. Lee and M. W. Cheng, "Intelligent control battery equalization for series connected lithium-ion battery strings," *IEEE Trans. Ind. Electron.*, vol. 52, no. 5, Oct. 2005, pp. 1297–1307.

[6] Y. S. Lee and G. T. Cheng, "Quasi-resonant zero-current-switching bidirectional converter for battery equalization applications," *IEEE Trans. Power Electron.*, vol. 21, no. 5, Sep. 2006, pp. 1213–1224.

[7] P. A. Cassani and S. S. Williamson, "Feasibility analysis of a novel cell equalizer topology for plug-in hybrid electric vehicle energy-storage systems," *IEEE Trans. Veh. Technol.*, vol. 58, no. 8, Oct. 2009, pp. 3938–3946.

[8] P. A. Cassani and S. S. Williamson, "Design, testing, and validation of a simplified control scheme for a novel plug-ion hybrid electric vehicle battery cell equalizer," *IEEE Trans. Ind. Electron.*, vol. 57, no. 12, Dec. 2010, pp. 3956–3962.

[9] T. H. Phung, A. Collet, and J. Crebier, "An optimized topology for next-to-next balancing of series-connected lithium-ion cells," *IEEE Trans. Power Electron.*, vol. 29, no. 9, Sep. 2014, pp. 4603–4613.

[10] C. Pascual and P. T. Krein, "Switched capacitor system for automatic series battery equalization," in Proc. *IEEE Appl. Power Electron. Conf. Expo.*, Feb. 1997, pp. 848–854.

[11] J. W. Kimball, B. T. Kuhn, and P. T. Krein, "Increased performance of battery packs by active equalization," in Proc. *IEEE Veh. Power Propulsion Conf.*, Sep. 2007, pp. 323–327.

[12] A. Baughman and M. Ferdowsi, "Double-tiered switched-capacitor battery charge equalization technique," *IEEE Trans. Ind. Appl.*, vol. 55, no. 6, Jun. 2008, pp. 2277–2285.

[13] M. Uno and H. Toyota, "Supercapacitor-based energy storage system with voltage equalizers and selective taps," in Proc. *IEEE Power Electron. Spec. Conf.*, Jun. 2008, pp. 755–760.

[14] M. Uno and H. Toyota, "Equalization technique utilizing series-parallel connected supercapacitors for energy storage system," in Proc. *IEEE Int. Conf. Sustainable Energy Technology*, Nov. 2008, pp. 999–1003.

[15] H. S. Park, C. H. Kim, K. B. Park, G. W. Moon, and J. H. Lee, "Design of a charge equalizer based on battery modularization," *IEEE Trans. Veh. Technol.*, vol. 58, no. 7, Sep. 2009, pp. 3216–3223.

[16] M. Uno and K. Tanaka, "Influence of high-frequency charge-discharge cycling induced by cell voltage equalizers on the life performance of lithium-ion cells," *IEEE Trans. Veh. Technol.*, vol. 60, no. 4, May 2011, pp. 1505–1515.

[17] Y. Yuanmao, K. W. E. Cheng, and Y. P. B. Yeung, "Zero-current switching switched-capacitor zero-voltage-gap automatic equalization system for series battery string," *IEEE Trans. Power Electron.*, vol. 27, no. 7, Jul. 2012, pp. 3234–3242.

[18] M. Y. Kim, C. H. Kim, J. H. Kim, and G. W. Moon, "A chain structure of switched capacitor for improved cell balancing speed of lithium-ion batteries," *IEEE Trans. Ind. Electron.*, vol. 61, no. 9, Aug. 2014, pp. 3989–3999.

[19] A. M. Imtiaz, F. H. Khan, and H. Kamath, "Time shared flyback converter" based regenerative cell balancing technique for series connected Li-ion battery strings," *IEEE Trans. Power Electron.*, vol. 28, no. 12, Dec. 2013, pp. 5960–5975.

[20] C. H. Kim, M. Y. Kim, H. S. Park, and G. W. Moon, "A modularized two-stage charge equalizer with cell selection switches for series-connected lithium-ion battery string in a HEV," *IEEE Trans. Power Electron.*, vol. 27, no. 8, Aug. 2012, pp. 3764–3774.

[21] C. H. Kim, M. Y. Kim, and G. W. Moon, "A modularized charge equalizer using a battery monitoring IC for series-connected Li-ion battery strings in electric vehicles," *IEEE Trans. Power Electron.*, vol. 28, no. 8, Aug. 2013, pp. 3779–3787.

[22] F. Baronti, G. Fantechi, R. Roncella, and R. Saletti, "High-efficiency digitally controlled charge equalizer for series-connected cells based on switching converter and upper-capacitor," *IEEE Trans. Ind. Informatics.*, vol. 9, no. 2, May 2013, pp. 1139–1147.

[23] N. H. Kutkut, D. M. Divan, and D. W. Novotny, "Charge equalization for series connected battery strings," *IEEE Trans. Ind. Appl.*, vol. 31, no. 3, May/Jun. 1995, pp. 562–568.

[24] N. H. Kutkut, H. L. N. Wiegman, D. M. Divan, and D. W. Novotny, "Charge equalization for an electric vehicle battery system," *IEEE Trans. Aerosp. Electron. Syst.*, vol. 34, no. 1, Jan. 1998, pp. 235–246.

[25] N. H. Kutkut, H. L. N. Wiegman, D. M. Divan, and D. W. Novotny, "Design considerations for charge equalization of an electric vehicle battery system," *IEEE Trans. Ind. Appl.*, vol. 35, no. 1, Jan. 1999, pp. 28–35.

[26] A. Xu, S. Xie, and X. Liu, "Dynamic voltage equalization for series-connected ultracapacitors in EV/HEV applications," *IEEE Trans. Veh. Technol.*, vol. 58, no. 8, Oct. 2009, pp. 3981–3987.

[27] J. Cao, N. Schofield, and A. Emadi, "Battery balancing methods: a comprehensive review," in Proc. *IEEE Veh. Power and Propulsion Conf.*, Sep. 2008, pp. 1–6.

[28] K. Z. Guo, Z. C. Bo, L. R. Gui, and C. S. Kang, "Comparison and evaluation of charge equalization technique for series connected batteries," in Proc. *IEEE Power Electron. Spec. Conf.*, Jun. 2006, pp. 1–6.

[29] M. Einhorn, W. Guertlschmid, T. Blochberger, R. Kumpusch, R. Permann, F. V. Conte, C. Kral, and J. Fleig, "A current equalization method for serially connected battery cells using a single power converter for each cell," *IEEE Trans. Veh. Technol.*, vol. 60, no. 9, Nov. 2011, pp. 4227–4237.

[30] M. Einhorn, W. Roessler. and J. Fleig, "Improved performance of serially connected Li-ion batteries with active cell balancing in electric vehicles," *IEEE Trans. Veh. Technol.*, vol. 60, no. 6, Jul. 2011, pp. 2448–2457.

[31] F. Mestrallet, L. Kerachev, J. Crebier, and A. Collet, "Multiphase interleaved converters for lithium battery active balancing," *IEEE Trans. Power Electron.*, vol. 29, no. 6, Jun. 2014, pp. 2874–2881.

[32] H. S. Park, C. E. Kim, C. H. Kim, G. W. Moon, and J. H. Lee, "A modularized charge equalizer for an HEV lithium-ion battery string," *IEEE Trans. Ind. Electron.*, vol. 56, no. 5, May 2009, pp. 1464–1476.

[33] C. H. Kim, H. S. Park, C. E. Kim, G. W. Moon, and J. H. Lee, "Individual charge equalization converter with parallel primary winding of transformer for series connected lithium-ion battery strings in an HEV," *J. Power Electron.*, vol. 9, no. 3, May 2009, pp. 472–480.

[34] S. H. Park, K. B. Park, H .S. Kim, G. W. Moon, and M. J. Youn, "Single-magnetic cell-to-cell charge equalization converter with reduced number of transformer windings," *IEEE Trans. Power Electron.*, vol. 27, no. 6, Jun. 2012, pp. 2900–2911.

[35] C. S. Lim, K. J. Lee, N. J. Ku, D. S. Hyun, and R. Y. Kim, "A modularized equalization method based on magnetizing energy for a series-connected lithium-ion battery string," *IEEE Trans. Power Electron.*, vol. 29, no. 4, Apr. 2014, pp. 1791–1799.

[36] M. Uno and K. Tanaka, "Single-switch cell voltage equalizer using multistacked buck–boost converters operating in discontinuous conduction mode for series-connected energy storage cells," *IEEE Trans. Veh. Technol.*, vol. 60, no. 8, Oct. 2011, pp. 3635–3645.

[37] M. Uno and K. Tanaka, "Double-switch single-transformer cell voltage equalizer using a half-bridge inverter and voltage multiplier for series-connected supercapacitors," *IEEE Trans. Veh. Technol.*, vol. 61, no. 9, Nov. 2012, pp. 3920–3930.

[38] M. Uno and A. Kukita, "Double-switch equalizer using parallel- or series-parallel-resonant inverter and voltage multiplier for series-connected supercapacitors," *IEEE Trans. Power Electron.*, vol. 29, no. 2, Feb. 2014, pp. 812–828.

[39] M. Uno and K. Tanaka, "Single-switch multi-output charger using voltage multiplier for series-connected lithium-ion battery/supercapacitor equalization," *IEEE Trans. Ind. Electron.*, vol. 60, no. 8, Aug. 2013, pp. 3227–3239.

[40] Y. H. Hsieh, T. J. Liang, S. M. Chen, W. Y. Horng, and Y. Y. Chung, "A novel high-efficiency compact-size low-cost balancing method for series-connected battery applications," *IEEE Trans. Power Electron.*, vol. 28, no. 12, Dec. 2013, pp. 5927–5939.

[41] S. West and P. T. Krein, "Equalization of valve-regulated lead-acid batteries: Issues and life test results," in Proc. *Int. Telecommun. Energy Conf.*, pp. 439–446, Sep. 2000.

Masatoshi Uno (M'06) was born in Japan in 1979. He received the B.E. degree in electronics engineering and the M.E. degree in electrical engineering from Doshisha University, Kyoto, Japan, in 2002 and 2004, respectively, and the Ph.D degree from the Graduate University for Advanced Studies, Kanagawa, Japan, in 2012.

Since 2004, he has been with Japan Aerospace Exploration Agency where he is currently a development researcher for spacecraft power systems. His research areas include switching power converters, cell equalizers, and life evaluation for supercapacitors and lithium-ion batteries, and development of fuel cell systems, for spacecraft power systems.

M. Uno is a member of the Institute of Electrical Engineering of Japan (IEEJ), and the Institute of Electronics, Information and Communication Engineers (IEICE).

Akio Kukita was born in Japan in 1967. He received the B.E. degree in physics from Chuo University, Japan, in 1993.

From 1993 to 1996 and 1996 to 2008, he was with SEIKO Holdings Corporation and Ebara Corporation, respectively. Since 2008, he has been with Japan Aerospace Exploration Agency as a senior engineer. His recent work has focused on the development of spacecraft power systems.